

COMMUNICATION

Framework flexibility-driven CO₂ adsorption on a zeolite

Hyun June Choi,^a Jung Gi Min,^a Sang Hyun Ahn,^a Jiho Shin,^a Suk Bong Hong,^{*a} Sambhu Radhakrishnan,^b C. Vinod Chandran,^b Robert G. Bell,^c Eric Breynaert^b and Christine E. A. Kirschhock^b

Received 00th xx 20xx,
Accepted 00th xx 20xx

DOI: 10.1039/xxxxxxxxxx

Adsorption of the greenhouse gas CO₂ by ordered porous materials, although cost-efficient and eco-friendly, has not yet achieved large-scale practical application. Here, we report that zeolite framework flexibility can be exploited by tuning a subtle interplay between extra-framework cations with framework oxygen and adsorbed guest molecule (CO₂). This phenomenon has been demonstrated on the Na⁺, K⁺ and Rb⁺ forms of the small-pore zeolite gismondine with a Si/Al ratio of 3.0, which show marked cation-dependent hystereses in their CO₂ isotherms. A detailed analysis of the structures by solid state NMR and XRD revealed the framework dynamics and the adsorption behavior is governed by the extraframework cations, which strive for coordination either with framework oxygen, guest molecules, or both. The K⁺ and Rb⁺ forms display very high CO₂ working capacities (2.8 and 3.0 mmol g⁻¹) for a 50:50 CO₂/CH₄ mixture under mild temperature swing conditions (25 - 100 °C at 1.0 bar), as well as high CO₂/CH₄ selectivities (36 and 28) at 25 °C. Given the excellent thermal and chemical stability of zeolites compared to other classes of adsorbents, and the here reported tuneable flexing action effected by the cations, zeolites displaying framework flexibility harbour great potential for fuel gas applications.

Solid-state, industrial-scale carbon capture and storage (CCS) requires porous materials, selectively absorbing CO₂ under ambient conditions in the presence of many other gases.^{1,2} For sustainability, this technology requires long-term durable materials with low-energy input for regeneration and CO₂ release.^{3,4} Compared to other classes of ordered porous materials,^{5,6} aluminosilicate zeolites have demonstrated high physicochemical stability in harsh industrial-scale processes.

New concepts

Zeolites? Already the Romans knew about those inorganic porous aluminosilicates, which today are omnipresent industrial catalysts and adsorbents. So what's new about them? Apparently they can be flexible, letting their charge compensating cations drive and control the dynamics of CO₂ adsorption and desorption. A detailed molecular level study, combining advanced solid state NMR with structure solution by powder X-ray diffraction, revealed CO₂ adsorption by flexible small pore zeolites can be finely tuned by selecting the correct extra-framework cations, yielding unexpected performance in CO₂ adsorption. The here reported mechanism is based on competition of guest molecules and framework oxygen for cation coordination. This in turn leads to astonishing framework deformation upon desorption and corresponding, fully reversible relaxation during adsorption. The stored deformation energy in desorbed state is released upon complexation of the cations by offered guest molecules, so that the conditions for adsorption and desorption can be precisely tuned to industrial requirements for temperature swing processing by choosing cations with varying affinity to framework oxygen on one, and adsorbate on the other hand. This discovery truly opens the view on unsuspected new horizons for smart uses of zeolites as adsorbents.

Gismondine, a small-pore zeolite with GIS topology, contains a three-dimensional (3D) pore system with two intersecting channels, consisting of 8-membered rings (8-MRs) of corner-sharing tetrahedral TO₄ units (T = Si or Al). The GIS framework can be constructed from laterally linked double-crankshaft chains (*dccs*) as composite building units (Movie S1, ESI[†]).^{7,8} Theoretical calculations using rigid, all-silica models have suggested this small-pore zeolite as a most promising candidate for CO₂ adsorption among known zeolites.⁹ However, GIS zeolites, typically synthesized with framework Si/Al ratios below 2.0,^{10,11} show negligible CO₂ uptake (< 0.03 mmol g⁻¹ at 25 °C and 1.0 bar).¹¹ We hypothesized that this may be due to the high number of charge compensating extra-framework cations blocking access to the 8-ring windows for CO₂ adsorption.

To first synthesize isostructural zeolites with lower number of extra-framework Na⁺ ions and thus higher framework Si/Al

^a Center for Ordered Nanoporous Materials Synthesis, Division of Environmental Science and Engineering, POSTECH, Pohang 37673, Korea.
E-mail: sbhong@postech.ac.kr

^b Center for Surface Chemistry and Catalysis, Characterisation and Application Team (COK-kat), Celestijnenlaan 200 F – box 2461, KU Leuven, 3001 Heverlee, Belgium

^c Department of Chemistry, University College London, 20 Gordon Street, London WC1H 0AJ, UK

[†] Electronic supplementary information (ESI) available. See DOI: 10.1039/xxxxxxxxxx

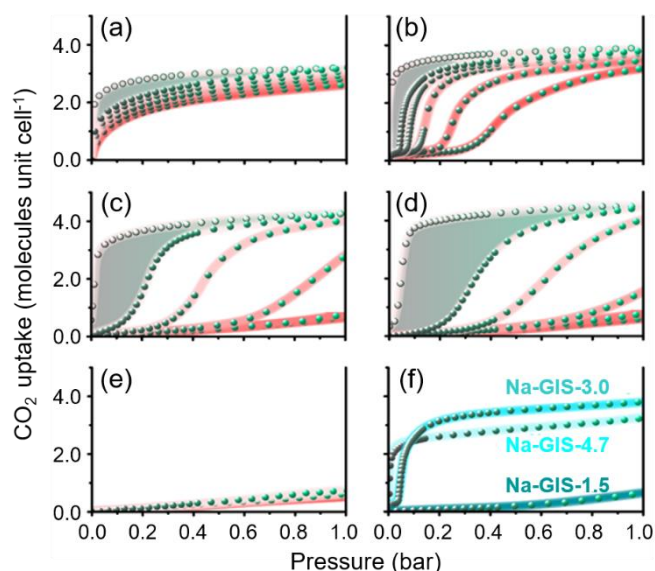


Fig. 1 Adsorption isotherms on (a) Li-, (b) Na-, (c) K-, (d) Rb-, and (e) Cs-GIS-3.0 as a function of CO₂ molecules per unit cell. Adsorption, filled symbols; desorption, open symbols. Red traces indicate measurement temperatures, from light to dark corresponding to 25, 35, 50, 60, and 75 °C. Green shaded areas show hysteresis between ad- and desorption at 25 °C. (F) Comparison of adsorption isotherms of Na-GIS-1.5 (dark), Na-GIS-3.0 (medium), and Na-GIS-4.7 (light).

ratios under wholly inorganic conditions, we carefully decreased the alkalinity of the synthesis mixture reported to give pure GIS materials with Si/Al ratios below 2.0,^{10,11} as well as increased crystallization temperature. This included the use of aluminosilicate gels with the composition $x\text{Na}_2\text{O}\cdot y\text{Al}_2\text{O}_3\cdot 10\text{SiO}_2\cdot 220\text{H}_2\text{O}$, where x and y are varied between $1.0 \leq x \leq 10.0$ and $0.5 \leq y \leq 2.0$, respectively (Table S1, ESI[†]). We were able to obtain Na-GIS-3.0 (the last number indicates the Si/Al ratio determined by elemental analysis) by heating a sodium aluminosilicate gel with Si/Al = 5.0 and Si/OH = 2.0 under rotation (60 rpm) at 150 °C for 3 days. It is worth noting that this 'organic-free, high-silica' GIS sample could be synthesized only over a narrow range of gel composition. We also synthesized ATMEANa-GIS-4.7 with a higher Si/Al ratio (4.7), using 2-amino-*N,N,N*-trimethylethanaminium (ATMEA) and Na⁺ ions as structure-directing agents by heating a gel with the oxide composition $4.5\text{ATMEA}\cdot 9.0\text{Na}_2\text{O}\cdot 1.0\text{Al}_2\text{O}_3\cdot 30\text{SiO}_2\cdot 1200\text{H}_2\text{O}$ at 150 °C for 7 days. For comparison, Na-GIS-1.5 was synthesized according to the procedure given elsewhere.^{10,11}

Powder X-ray diffraction (PXRD) measurements on as-synthesized Na-GIS-1.5, Na-GIS-3.0, and Na-GIS-4.7 reveal that these GIS zeolites are highly crystalline and phase-pure (Fig. S1, ESI[†]). Scanning electron microscopy (SEM) images show that all of them are characterized by aggregated ill-defined plate-like morphologies and similar crystallite sizes (*ca.* 0.5–2.0 μm in width). ²⁷Al MAS NMR spectra of as-synthesized Na-GIS-1.5, Na-GIS-3.0, and Na-GIS-4.7 exhibit only one prominent resonance at 55–60 ppm, typical of tetrahedral Al, while the ²⁹Si MAS NMR spectra indicate framework Si/Al ratios of 1.5, 3.0, and 4.7, respectively, in full agreement with their bulk Si/Al ratios determined by elemental analysis (Fig. S3 and Table S2, ESI[†]). It is remarkable that unlike Na-GIS-1.5, the latter two zeolites with higher Si/Al ratios maintain the structural integrity after heating

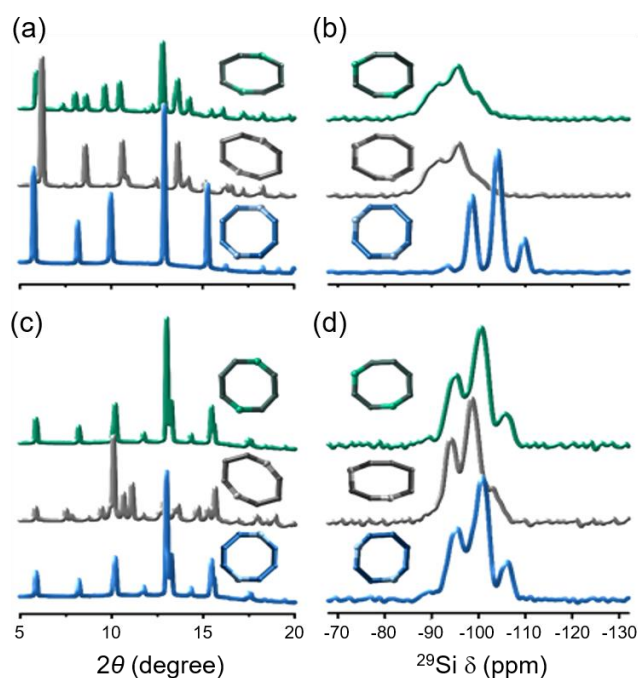


Fig. 2 PXRD patterns (left) and ²⁹Si MAS NMR spectra (right) of (a) and (b) Na-GIS-3.0 and (c) and (d) Rb-GIS-3.0 in hydrated (blue), dehydrated (gray), and CO₂-loaded (green) states. Also shown are the 8-MR windows of the GIS framework as seen in crystallographic a and b directions with Al positions highlighted.

at 550 °C for 5 h, which is also the case of stirring in acidic (pH = 3–5) conditions for 24 h (Fig. S4 and S5, ESI[†]), suggesting that their high thermal and chemical stability.

The Al content of the GIS framework was found to strongly impact CO₂ adsorption behavior (Fig. 1): comparing the Na⁺ form of GIS zeolites with different Si/Al ratios, the highest CO₂ uptake (3.7 mmol g⁻¹ at 25 °C and 1.0 bar) was observed for Na-GIS-3.0. The uptakes on Na-GIS-1.5 and Na-GIS-4.7 were 0.6 and 3.0 mmol g⁻¹, respectively. Most interestingly, and unlike the common Langmuir-like CO₂ adsorption by Na-GIS-4.7 (Fig. S15, ESI[†]), sorption by Na-GIS-3.0 exhibits hysteretic behavior and a step around 0.05 bar (Fig. 1b). This is exceptional for CO₂ adsorption by zeolitic materials.^{12,13} The type of the extra-framework cations was also found to determine the adsorption properties (Fig. 1 and Fig. S6 and Table S2, ESI[†]). Over the studied temperature range (25–75 °C), CO₂ adsorption on Li-GIS-3.0 follows a Langmuir isotherm, whereas Cs-GIS-3.0 adsorbs negligibly, probably due to steric hindrance by the large Cs⁺ ions. Isotherms of all other alkali exchanged GIS-3.0 zeolites show clear hystereses. The onset pressure of the step at 25 °C, as well as the area of the hysteresis loop, increases in the order Na-GIS-3.0 < K-GIS-3.0 < Rb-GIS-3.0, with uptakes of roughly one CO₂ molecule per alkali cation at 25 °C and 1.0 bar (Fig. 1b–d). CO₂ adsorption on these zeolites reaches equilibrium within 5 min (Fig. S16, ESI[†]), with isosteric heats of adsorption at low coverages in the physisorption range (40–45 kJ mol⁻¹) (Fig. S17 and S18, ESI[†]).

The effects of dehydration and CO₂ adsorption on the structures of Na-, K-, and Rb-GIS-3.0 zeolites were elucidated by NMR crystallography, combining solid-state NMR with PXRD. Local interactions of guest molecules with the extra-framework

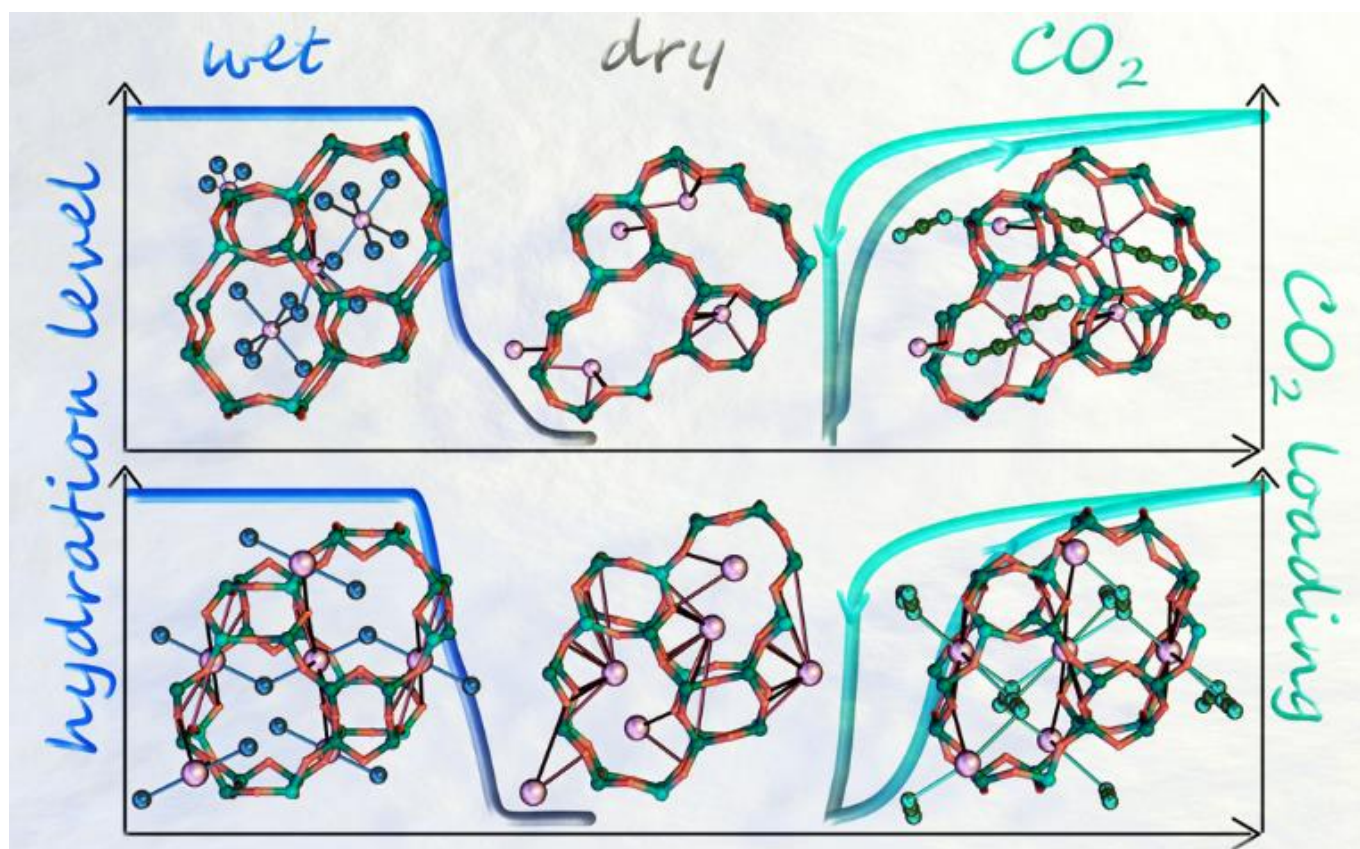


Fig. 3 The structures of Na-GIS-3.0 (top) and Rb-GIS-3.0 (bottom) in hydrated (left), dehydrated (middle) and CO₂-loaded (right) states. The blue and green traces represent thermogravimetric dehydration and CO₂ adsorption–desorption isotherms, respectively.

cations and/or the zeolite framework can be probed by solid-state NMR, while global structural changes are monitored by PXRD and Rietveld analysis.

In as-synthesized, hydrated state, Na-GIS-3.0 appears on first sight highly crystalline, with well-resolved PXRD pattern and ²⁹Si MAS NMR signals (Fig. 2 and Table S5, ESI[†]). The 1D ²⁷Al MAS NMR spectrum of hydrated Na-GIS-3.0 shows one sharp and symmetric line with an isotropic chemical shift (δ_{iso}) of 60.3 ppm, indicating a single, locally symmetric ²⁷Al environment, as confirmed by ²⁷Al triple-quantum MAS NMR (Fig. S8, ESI[†]). Interestingly, the 1D ²³Na MAS spectrum of the same zeolite suggests the presence of two Na⁺ environments (Fig. S9, ESI[†]) in equal occupation. These results clearly indicate the ordering of Na⁺ ions, also implying an ordering of framework Al atoms in this zeolite. Thus, although the PXRD pattern of hydrated Na-GIS-3.0 could be indexed in a tetragonal space group, a lower symmetry had to be considered (see discussion of choice of space group in the ESI[†]). A structure description consistent with PXRD and solid-state NMR is possible for all investigated structures in the monoclinic space group *P2₁/n*, yielding one site for Al throughout, but two sites with almost equal occupancies for Na⁺. While the first Na⁺ site is located within 8-MR windows with two opposing Al atoms, the second site is positioned within 8-MRs, where the Al atoms are separated by two Si atoms on one, and four on the other side. (Fig. 3 and Movie S2, ESI[†]). In the former type of 8-MR windows, Na⁺ is centred and octahedrally coordinated by six water molecules. In the latter window-type, Na⁺ is slightly off-center and within interaction

distance to framework oxygen atoms. Globally, this results in the formation of chains of corner-sharing [H₂O–Na⁺] ↔ H₂O ↔ [Na⁺–(framework+H₂O)] octahedra.

The PXRD pattern and solid-state NMR spectra of hydrated Na-GIS-3.0, drastically but fully reversibly, change upon dehydration and subsequent exposure to CO₂ (Fig. 2 and Fig. S10 and S11, ESI[†]). The ²⁹Si MAS NMR signals strongly shift downfield, losing resolution, while the ²⁷Al and ²³Na lines broaden and become increasingly asymmetric (Fig. S12, ESI[†]). This indicates structural changes without framework degradation, consistent with the high flexibility of the GIS topology predicted theoretically.¹⁴ The PXRD pattern of fully dehydrated Na-GIS-3.0 can be clearly indexed in space group *P2₁/n* (Table S6, ESI[†]). Compared to the fully hydrated, quasi-tetragonal sample, its framework is significantly distorted, and the Na⁺ ions are strongly shifted towards the framework onto crystallographically different sites. The quadrupolar ²³Na and ²⁷Al nuclei sensitively probe electric field gradients (EFG) and thus the charge distribution in pore space and framework of Na-GIS-3.0, respectively. Upon losing their coordinating water molecules, the Na⁺ ions move from the 8-MR windows into the pockets of the *dcc* units, compressing them significantly (Fig. 3 and Movie S2, ESI[†]). Owing to the non-random Al distribution in Na-GIS-3.0, these pockets are identical neither crystallographically, nor in terms of charge distribution.

Exposing dehydrated Na-GIS-3.0 to CO₂, the local environments of framework Al atoms and extra-framework Na⁺ ions become slightly more symmetrical again, yielding

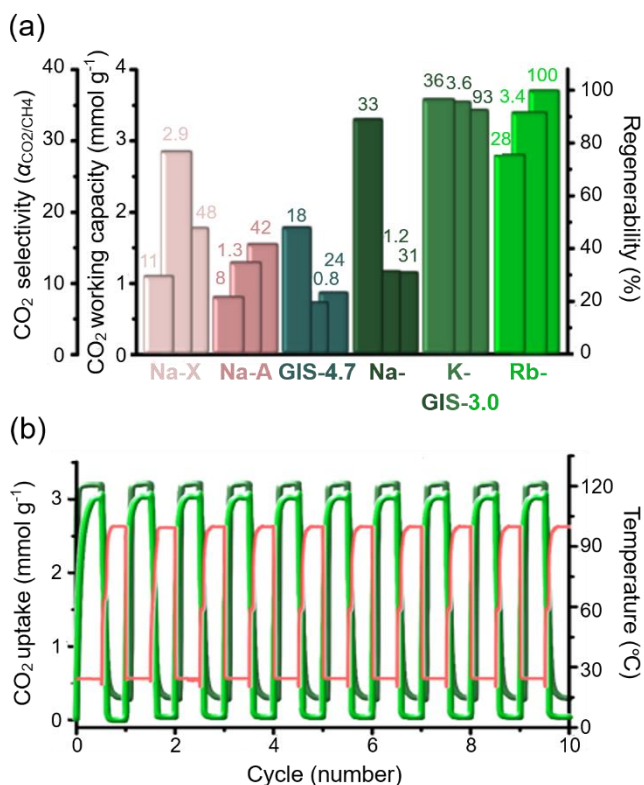


Fig. 4 (a) CO₂ Selectivity (α), CO₂ working capacity, and regenerability in columns (from left to right) of Na-X, Na-A, Na-GIS-4.7, Na-GIS-3.0, K-GIS-3.0, and Rb-GIS-3.0. (b) CO₂ adsorption-desorption cycles for K-GIS-3.0 (dark green) and Rb-GIS-3.0 (light green) with adsorption at 25 °C using a 50:50 CO₂/CH₄ mixture and desorption at 100 °C using pure CO₂.

sharpened ²³Na and ²⁷Al MAS NMR spectra (Fig. S12, ESI[†]). Interestingly, the ²⁹Si MAS NMR spectrum shows little change (Fig. 2b), revealing that the overall framework has only marginally relaxed upon CO₂ adsorption. Structural analysis by PXRD confirms that Na⁺ is now at an interaction distance to adsorbed CO₂ molecules, but still in contact to the framework oxygen atoms (Fig. 3 and Table S7 and Movie S2, ESI[†]): while interaction with CO₂ causes one of the two Na⁺ sites to return to the centre of a still compressed 8-MR window, the Na⁺ ions on the other site only move slightly from their *dcc* pocket. Na⁺ ions on both positions are now at interaction distance to the same CO₂ site, resulting in chains of [framework-Na⁺] \leftrightarrow CO₂ \leftrightarrow [Na⁺-framework].

We next examined the effect of dehydration and CO₂ adsorption on the structures of K- and Rb-GIS-3.0 zeolites. The downfield shifts of ²⁹Si and ²⁷Al signals during dehydration decrease with increasing size and softness of extra-framework cations (Fig. 2 and Fig. S11 and S13, ESI[†]), indicating the frameworks of K- and Rb-GIS-3.0 distort less upon water removal, compared to the Na⁺ form. The line shape of the ²⁹Si MAS NMR spectrum of CO₂-loaded K-GIS-3.0 lies between the spectra of hydrated and dehydrated states, while the spectra of CO₂-loaded and hydrated Rb-GIS-3.0 samples are virtually identical, implying partial relaxation of the former and full relaxation of the latter. The NMR observations match well with the PXRD results: in contrast to Na⁺, both K⁺ and Rb⁺ ions were

located on single crystallographic sites with 100% occupancy after dehydration and CO₂ loading (Fig. 3 and Tables S8-S13 and Movie S2, ESI[†]) in accordance with the lack of splitting of their ²⁷Al and ⁸⁷Rb MAS NMR signals (Fig. S9 and S13, ESI[†]). K⁺ ions, as well as Rb⁺ ions, occupy the centres of 8-MRs in their hydrated state, being coordinated to four framework oxygen atoms, each. Water molecules are found between the cations, leading to infinite chains of distorted octahedra. Similar to Na-GIS-3.0, K⁺ and Rb⁺ move upon dehydration from the 8-MR windows closer to the framework, but show clear preference for channel crossings, close to one of the two *dcc* pocket types. The distortion of the framework is smaller with increasing cation size and softness, reflecting the lower oxophilicity and thus the longer oxygen-cation bond lengths. The presence of CO₂ results in return of the cations to positions similar as in the hydrated state, the centres of 8-MR windows with CO₂-connecting neighbouring cations, instead of water molecules.

The maximum working capacity of zeolites as CO₂ adsorbents is typically obtained in a vacuum swing adsorption (VSA) cycle suffering from high energy penalties associated with large-volume vacuum applications. However, with materials allowing CO₂ desorption at suitably low temperatures, a temperature swing adsorption (TSA) cycle can compete with, and even outperform current VSA cycling.¹⁵ The structural characterization revealed that, unlike most microporous CO₂ adsorbents, retaining CO₂ by non-specific dispersion forces, GIS-3.0 absorbs CO₂ via specific interaction between its alkali cations and CO₂. In this mechanism guest molecules compete with the framework oxygen for cation coordination, which strongly affects the framework dynamics and ad- and desorption behaviour of the zeolite. This allows fine tuning of the adsorbent properties by choosing the cation with the most suitable size, softness, and affinity for a given adsorbate. The ease with which K⁺ and Rb⁺ changes between the solvation by oxygen of the distorted framework and the solvation by CO₂ in the loaded and more relaxed state (Fig. 3 and Fig. S14 and Movie S2, ESI[†]) makes K- and Rb-GIS-3.0 particularly attractive candidates for TSA. To assess their potential, adsorption at 25 °C and desorption at 75 - 150 °C of pure CO₂ at 1.0 bar was performed and compared to well-known zeolite adsorbents Na-A (LTA; Si/Al = 1.0) and Na-X (FAU; Si/Al = 1.3), as well as to Na-GIS-3.0 and Na-GIS-4.7 (Fig. 4a and Fig. S19, ESI[†]). At 75 °C K-GIS-3.0 and Rb-GIS-3.0 hardly desorbed CO₂, owing to the hystereses of the isotherms. But increasing the desorption temperature from 75 °C to 100 °C led to excellent regenerability (93% and 100%, respectively), whereas the restoration of the other four zeolites remained below 50%. A further increase of temperature to 125 °C allowed K-GIS-3.0 to fully desorb CO₂. Consequently, the CO₂ working capacities (3.6 and 3.4 mmol g⁻¹, respectively) of K- and Rb-GIS-3.0 over the temperature interval 25 to 100 °C exceed even the working capacity (2.8 mmol g⁻¹) of the large-pore zeolite Na-X (Fig. 4a and Fig. S19, ESI[†]).

We also evaluated the performance of K- and Rb-GIS-3.0 for separation of CO₂ and CH₄ by adsorbing a 50:50 mixture at 25 °C, which then desorbs pure CO₂ at 100 °C (Fig. 4b). Both zeolites showed large working capacities (2.8 and 3.0 mmol g⁻¹,

respectively), together with outstanding stability over repeated TSA cycles under dynamic conditions. Converted to the weight percentage, their working capacities (12–13 wt%) are comparable with the CO₂ working capacities (10–15 wt%) of a series of *N,N'*-dimethylethylenediamine-M₂(4,4'-dioxidobiphenyl-3,3'-dicarboxylate) compounds, where M is Mg, Mn, Fe, Co or Zn, the best CO₂ metal-organic framework adsorbents under TSA process.^{16,17} We also found that CO₂/CH₄ selectivities (36 and 28, respectively) are considerably larger than the selectivities (8 and 11, respectively) observed for Na-A and Na-X, which is also the case for CO₂/N₂ separation (Fig. S20 and S21 and Table S14, ESI[†]). However, both K- and Rb-GIS-3.0 zeolites showed negligible CO₂ uptake when evaluated in presence of small amounts (3%) of water (Fig. S22, ESI[†]), in line with their strong hydrophilicity, hinting at their large potential for drying applications, as well as for upgrading of dried natural gas and biogas.

Conclusions

In summary, our study demonstrates not only that zeolites can show exceptional flexibility, but also that their pore space is efficiently controlled by the physicochemical properties of the extra-framework cations. The latter are subject to the Al distribution in the zeolite framework and compel guest molecules such as water and carbon dioxide to compete with framework oxygen atoms for their complexation. This provides a wholly new toolbox to tailor the properties of zeolites to specific applications like sustainable CO₂ separation.

Author contributions

S. B. H. conceived and supervised the research project. H. J. C., J. S., and S. H. A. carried out zeolite synthesis and characterization. H. J. C. and J. G. M. conducted gas sorption experiments. C. E. A. K., E. B., R. G. B., V. C., and S. R. performed NMR crystallography, including solid-state NMR, PXRD analysis, and related modelling. H. J. C., E. B., C. E. A. K., and S. B. H. co-wrote the paper. All authors discussed the results and commented on the manuscript.

Conflicts of interest

POSTECH (co-inventors S. B. H. and H. J. C.) filed for a patent that relates to the synthesis and CO₂ adsorption properties of GIS-3.0 zeolites.

Acknowledgements

This work was supported by National Research Foundation of Korea grants (2012R1A3A-2048833 and 2018K2A9A1A-06070020), Flanders Research Foundation, Flemish Government, and European Union's Horizon 2020 research grant (834134). We thank M. Choi and C. Kim (KAIST) for the dry cycling experiments and PAL for synchrotron diffraction

experiments at beamlines 9B (D. Ahn and Y. H. Jung) and 2D (D. Moon). PAL is supported by MSIP and POSTECH.

Notes and references

- 1 E. S. Sanz-Pérez, C. R. Murdock, S. A. Didas and C. W. Jones, *Chem. Rev.* 2016, **116**, 11840.
- 2 G. T. Rochelle, *Science* 2009, **325**, 1652.
- 3 B. Wang, A. P. Côté, H. Furukawa, M. O'Keeffe and O. M. Yaghi, *Nature* 2008, **453**, 207.
- 4 M. Palomino, A. Corma, F. Rey and S. Valencia, *Langmuir* 2010, **26**, 1910.
- 5 A. G. Slater and A. I. Cooper, *Science* 2015, **348**, aaa8075.
- 6 K. Sumida, D. L. Rogow, J. A. Mason, T. M. McDonald, E. D. Bloch, Z. R. Herm, T.-H. Bae and J. R. Long, *Chem. Rev.* 2012, **112**, 724.
- 7 K. Fischer and V. Schramm, *Adv. Chem. Ser.* 1971, **101**, 250.
- 8 Ch. Baerlocher and L. B. McCusker, Database of Zeolite Structures: <http://www.iza-structure.org/databases/> (Accessed February 21, 2020).
- 9 M. Fischer and R. G. Bell, *J. Phys. Chem. C* 2012, **116**, 26449.
- 10 W. C. Beard, *Adv. Chem. Ser.* 1971, **191**, 237.
- 11 M. D. Oleksiak, A. Ghorbanpour, M. T. Conato, B. P. McGrail, L. C. Grabow, R. K. Motkuri and J. D. Rimer, *Chem. Eur. J.* 2016, **22**, 16078.
- 12 M. M. Lozinska, E. Mangano, J. P. S. Mowat, A. M. Shepherd, R. F. Howe, S. P. Thompson, J. E. Parker, S. Brandani and P. A. Wright, *J. Am. Chem. Soc.* 2012, **134**, 17628.
- 13 V. M. Georgieva, E. L. Bruce, M. C. Verbraeken, A. R. Scott, W. J. Casteel, Jr., S. Brandani and P. A. Wright, *J. Am. Chem. Soc.* 2019, **141**, 12744.
- 14 V. Kapko, C. Dawson, M. M. J. Treacy and M. F. Thorpe, *Phys. Chem. Chem. Phys.* 2010, **12**, 8531.
- 15 N. Hedin, L. Andersson, L. Bergström and J. Yan, *Appl. Energy* 2013, **104**, 418.
- 16 J. A. Mason, K. Sumida, Z. R. Herm, R. Krishna, J. R. Long, *Energy Environ. Sci.* 2011, **4**, 3030.
- 17 T. M. McDonald, J. A. Mason, X. Kong, E. D. Bloch, D. Gygi, A. Dani, V. Crocella, F. Giordanino, S. O. Odoh, W. S. Drisdell, B. Vlaisavljevich, A. L. Dzubak, R. Poloni, S. K. Schnell, N. Planas, K. Lee, T. Pascal, L. F. Wan, D. Prendergast, J. B. Neaton, B. Smit, J. B. Kortright, L. Gagliardi, S. Bordiga, J. A. Reimer, J. R. Long, *Nature* 2015, **519**, 303.